Hindawi
Science and Technology of Nuclear Installations
Volume 2018, Article ID 8989070, 12 pages
https://doi.org/10.1155/2018/8989070

*Research Article*

# Large Scale Experiments Representing a Containment Natural Circulation Loop during an Accident Scenario

**R. Kapulla**[1], **G. Mignot**[2], **S. Paranjape**[1], **M. Andreani**[3] and **D. Paladino**[1]

[1]*Laboratory for Reactor Physics and Thermal-Hydraulics, Paul Scherrer Institut, 5232 Villigen, Switzerland*
[2]*Oregon State University, 1500 SW Jefferson St., Corvallis, OR 97331, USA*
[3]*Laboratory for Simulation and Modelling, Paul Scherrer Institut, 5232 Villigen, Switzerland*

Correspondence should be addressed to R. Kapulla; ralf.kapulla@psi.ch

Received 9 May 2018; Accepted 30 July 2018; Published 1 November 2018

Academic Editor: Hidemasa Yamano



The assessment of hydrogen release, distribution, and mitigation measures in the containment of a nuclear power plant is increasingly based on code calculations. These calculations require state-of-the-art experiments to benchmark the codes against them. Two of these experiments are presented in this paper. These experiments were conducted in the PANDA facility (Switzerland) in the framework of the OECD/NEA HYMERES project. The experiments consider natural circulation flow in a two-room type containment where flow loops can form between the inner and the outer zones. During normal operation these zones are separated and in the case of an accident they become either connected by the opening of rupture disks, convective foils, and dampers or connected by bursting of doors and opening of other connections between compartments. For the experiments considered here one lower PANDA-vessel represents the steam generator (SG) tower and the inaccessible area whereas the other vessel represents the outer room area. The lower vessels are isolated from one another except for a small aperture that represents the damper. The two upper vessels—representing the containment dome—are connected to the lower vessels through tubes. The scenario consisted of four phases. In phase 1, a high steam mass flow rate was injected in the vessel representing the SG tower. After the relaxation phase 2, helium (representing hydrogen) was injected in the same vessel (phase 3). Finally in phase 4 no active interventions were done until the end of the test. Two tests were conducted to evaluate the developing helium transport by the natural circulation flow: one with and one without damper (by closing the aperture). The results showed that a two-room containment (TRC) mixing scenario can be well represented with the PANDA facility. It is found that, with the mixing damper open, a global natural circulation loop develops over all four vessels, whereas with closed damper the natural circulation loop is established only between the three vessels representing the inner zone and the upper dome. It is shown that the presence of the damper has a strong effect on the resulting helium content in the inner zone with 3 times less helium at the end of the test compared with the configuration without damper. The formation of a stable helium stratification in the upper vessels was observed in the presence of the open damper.

## 1. Introduction

The thermal-hydraulic processes during a postulated severe accident in a nuclear power plant are very complex. The associated physical phenomena such as high velocity jets at the break location, large plumes impinging on internal structures, condensation, and reevaporation of steam as well as hydrogen and aerosol release and transport result in a large variety of length and velocity scales which are apparently challenging for code calculations either with Lumped Parameter (LP) or with Computational Fluid Dynamics (CV) codes, Andreani et al. [1]. The HYMERES project (Hydrogen Mitigation Experiments for Reactor Safety) was launched to improve the understanding of the hydrogen mixing phenomena in containments to enhance the modeling in support of safety assessments that will be performed for current and new nuclear power plants, OECD-NEA [2]; Visser et al. [3]. Within the HYMERES project, one test series (HP6) was dedicated to the study of the formation and sustainability of large natural circulation loops expected to build-up in the containment as a consequence of the opening of designed apertures typical of two-room type containments. Prominent

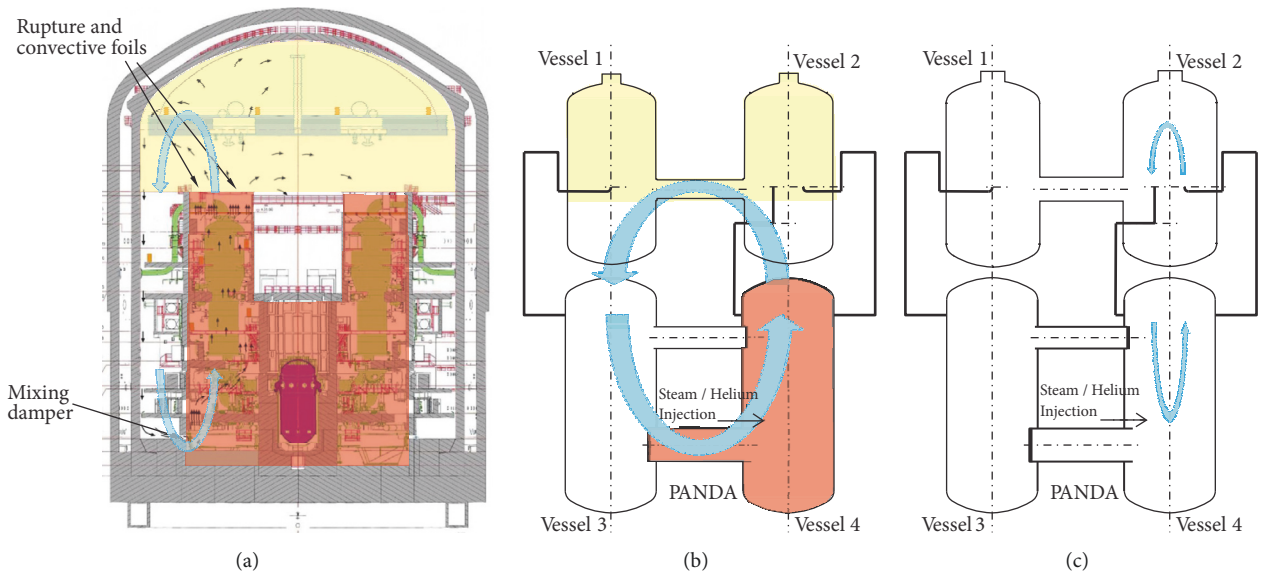


Figure 1: Two-room containment concept as implemented in an EPR™ (a) with prevailing convection loop and corresponding configuration of the PANDA facility (b) during the final state of the experiment HP6_1 and natural circulation loop for the KONVOI type containment (c) for experiment HP6_2. Corresponding areas have the same color. Picture on the left taken from Dimmelmeier et al. [4].

examples of the two-room type containments can be found in the KONVOI and the EPR™ reactor type. One room comprises the reactor pressure vessel, the steam generators, and the primary circuit in the so-called "inaccessible area", Figure 1 (red shaded area), while the second part consists of all the surrounding volumes of the containment which are "accessible" during normal operation, Figure 1 (yellow and white shaded area). As part of the hydrogen mitigation strategy, the passive CONVECT system was implemented to act under severe accident conditions.

The CONVECT system consists of rupture and convective foils located on the upper part of the steam generator tower and a mixing damper between the inner room and the surrounding accessible area which transforms the two-room into a one-room containment ensuring the mobilization of larger gas volume to dilute the released hydrogen, Dimmelmeier et al. [4]. A representation and color coded comparison of the expected prevailing convection loops in the EPR™ two-room containment and the PANDA facility are depicted in Figure 1.

The KONVOI type containment is not equipped with mixing dampers, but with rupture disks at the top of the steam generator towers. In case of a postulated accident the rupture disks open and complex natural circulation loops results, Figure 1(c). We report here of two tests conducted in the PANDA facility within the HYMERES HP6 series, namely, HP6_1 and HP6_2. The HP6_1 test has similarity with an EPR™ two-room containment and HP6_2 is similar to a KONVOI type containment. However, both experiments are not intended to address the reactor concepts directly, but the specific designs were only considered to obtain some meaningful figures for the main geometrical data, reasonable severe accident sequences from open literature and to derive a generic two-room containment concept Andreani et al. [5]. Based on extensive preliminary calculations by Andreani et al. [5] the objectives of the HP6 series were twofold: to reproduce as much as possible the main features of the containment response for these idealized accident scenarios and to create an experimental database suitable for the assessment of advanced computational tools (e.g., Lumped Parameters (LP), 3D-type codes and CFD codes) for the analysis of the flow transport in a multicompartment containment. However, some of the axis scales in the figures of the present paper are presented in nondimensional form, because the data of the OECD HYMERES project belongs to the project participants. The full set of HYMERES experimental data will be opened for the public in 2020. Moreover, if the reader is from one of the HYMERES participating countries and would like to analyse the PANDA HP6 tests with computational tools, he/she could contact the project representative Organization in his/her own Country and/or the OECD/NEA to obtain additional information related to the HYMERES PANDA HP6 tests and project documents. Nevertheless, the present overview should allow the reader to follow and understand the main phenomena characterizing the HP6 test series.

## 2. PANDA Facility and Test Scenario

PANDA is a large scale thermal-hydraulic facility designed to investigate containment system behavior and related phenomena for different ALWR designs, e.g., SBWR or ESBWR as well as for large scale separate effect tests. PANDA was used in the past for various investigations, Kelm et al. [6]; Kapulla et al. [7, 8]; Paladino et al. [9]; Papini et al. [10]; Visser et al. [3]; Filippov et al. [11]. The overall height of the PANDA facility is 25 m, the total volume of the vessels is about 460 $m^3$, and the maximum operating conditions

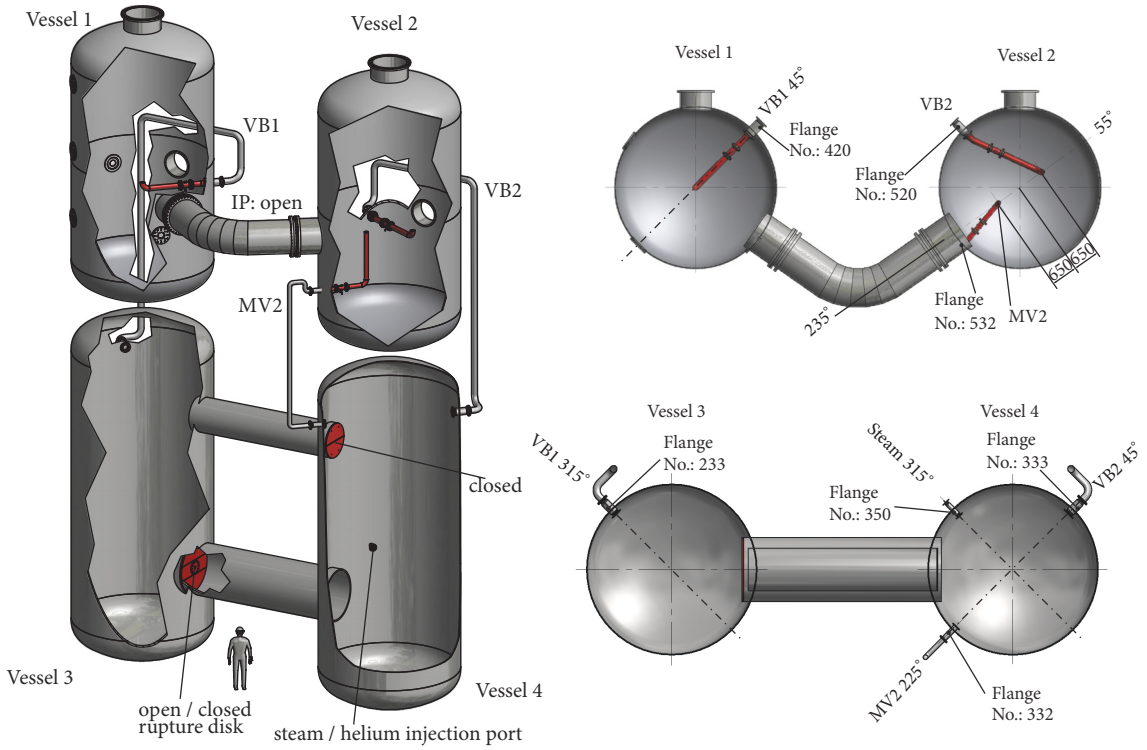


Figure 2: Different views of the four PANDA vessels illustrating the configuration and the pipes between the vessels as used for the HP6 series. A 3D view is shown on the left and a horizontal cross section through Vessels 1 and 2 at the top and horizontal cross section through Vessels 3 and 4 at the bottom on the right side.

are 10 bar at 200°C. The facility is equipped with electrical heaters with a maximum power of 1.5 MW which is used to produce steam for the preconditioning of the facility and to perform the tests. Various auxiliary systems are available to maintain and control the necessary initial and boundary conditions during the tests. The PANDA instrumentation covers the measurement of fluid and wall temperatures, absolute and differential pressures, flow rates, heater power, and gas concentrations. The measurement sensors are installed in all facility components, in the system lines, and in the auxiliary systems.

The experiments address the flow and the gas distribution in a generic two-room configuration which can be found in various reactor designs such as the equipment room and outer zone of the EPR™ which are not connected under normal operation conditions or the fuel machine vault/pump room of a PHWR Andreani et al. [5]. Scaling issues such as the ratio between the volume of the inaccessible area and the total volume in the two-room concept should be approximately reproduced in the tests in PANDA are covered and discussed in Andreani et al. [5]. In the two-room concept, natural circulation is established in a LOCA accident scenario between the inner rooms (inaccessible area) and the outer containment, following the opening of rupture and convective foils (constituting the Pressure Equalization Ceiling, PEC), as well as dampers (Figure 1 as well as Andreani et al. [5] and Dimmelmeier et al. [4]). The expected flow path is depicted in Figure 1(b) with upwards flow through the foils in the broken loop, downward flow along the containment wall and flow through the dampers. Additionally, secondary flows are produced between the broken and the intact loops. In general, the convection loops will be affected by the operation of other equipment, such as PARs or spray.

*2.1. PANDA Instrumentation and Configuration.* For the experiments under consideration all 4 vessels of the PANDA facility were used to represent a generic two-room containment configuration as presented above in Figure 1. A 3D view of the PANDA facility with the pipes connecting the vessels is given in Figure 2. The vessels at the top (Vessels 1 and 2) have an inner diameter of 4 m each and a height of 8 m whereas the bottom vessels (Vessels 3 and 4) have also a diameter of 4 m but are 11 m tall. For both experiments Vessel 4 represents the room with the break location, i.e., steam and helium (the substitute for hydrogen) are injected in Vessel 4. Two blind flanges (depicted in red in Figure 2) were installed at the interconnecting pipes to isolate Vessel 4 from Vessel 3.

The lower flange was either equipped with an 80 mm diameter aperture in its center to mimic the opening of a damper (HP6_1) or completely closed (HP6_2). Vessels 1 and 2 represent the upper dome of the containment in a two-room concept (see Figure 1). With the damper open or closed, the upper vessels represent a large single volume and the 970 mm diameter interconnecting pipe was left open. Upper and lower vessels were connected through already existing lines, namely, Vacuum Breaker line 1 and 2 (VB1 and

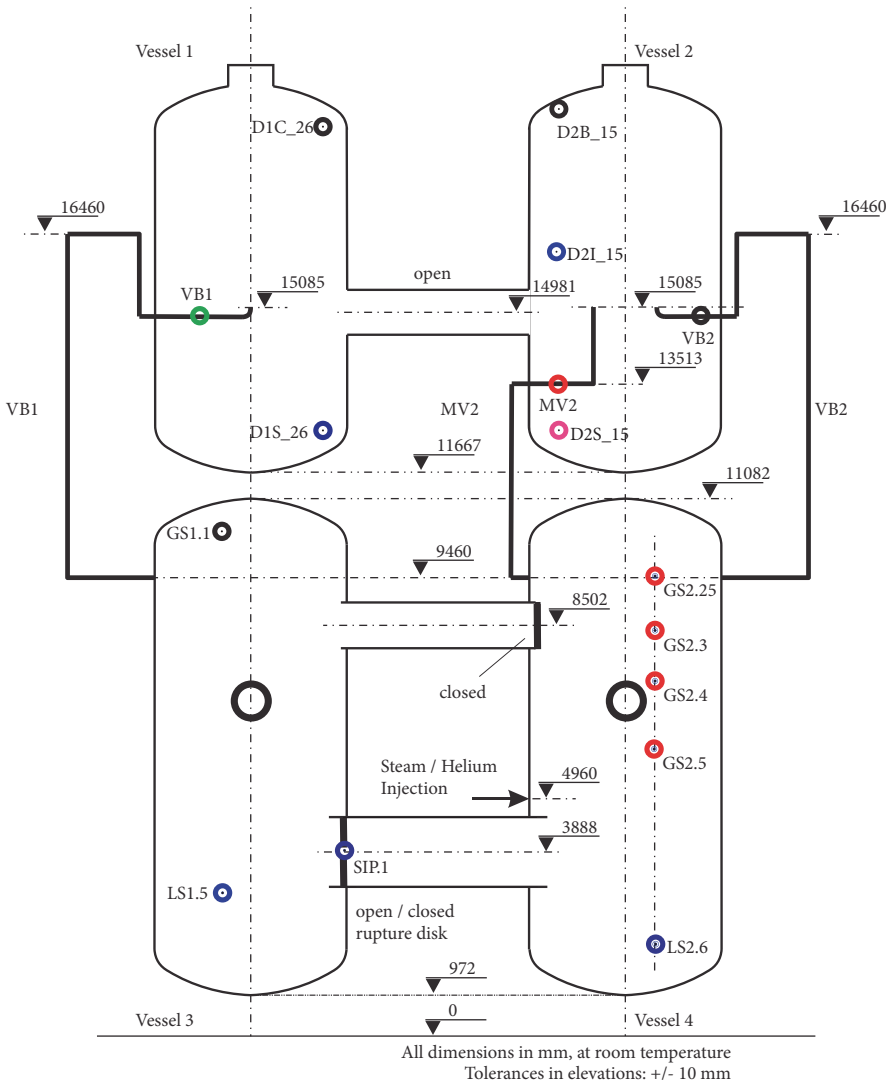


Figure 3: Four PANDA vessels with the main elevations of the pipes connecting the vessels and with selected concentration and temperature measurement positions depicted as circles.

VB2) and Main Vent line 2 (MV2). The use of the lines was supported by extensive scoping calculations conducted with GOTHIC Andreani et al. [5] which confirmed the formation of a natural circulation loop mobilizing the full height of the facility in the HP6 test scenario. The VB lines have an inner diameter of 134 mm whereas the MV2 line has an inner diameter of 109 mm. All line outlets were located at the same elevation, 15085 mm above ground in Vessels 1 and 2 slightly higher than the middle elevation of the interconnecting pipe, Figure 3. The line inlets in Vessel 3 and 4 were located at the same elevation 9460 mm above ground. For a better observation of the flow in the upper vessels the pipe outlet of VB2 is oriented at 55° and the outlet of MV2 at 235° in Vessel 2 and the inlet of VB1 at 45° in Vessel 1, respectively (Figure 2), because these planes already contained a dense thermocouple instrumentation, i.e., 110 and 50, respectively. Great care was also taken to choose the path of the capillary lines used to measure the gas concentration in each vessel in order to avoid any possible in-line condensation during the test. The positions of the relevant concentration and temperature measurement used for the experiment are depicted in Figure 3. The uncertainty of the thermocouples is 1.5°C while the gas concentration measurement uncertainty is estimated at 1.5% relative.

*2.2. Test Procedure.* The scenario for the PANDA experiments consisted for both experiments of four phases. The facility was preconditioned with air at ambient temperature and pressure. During phase 1, a high steam flow rate was injected into Vessel 4 for 5100 s and time zero depicts the start of the steam injection. This is the start of the experiment and corresponds to time zero. After a relaxation phase of 3000 s (phase 2) helium was injected during phase 3 in the same Vessel 4 for 580 s. Finally (phase 4) the system remained untouched until the end of the experiment. The only difference between the two tests is the presence (HP6_1) or absence

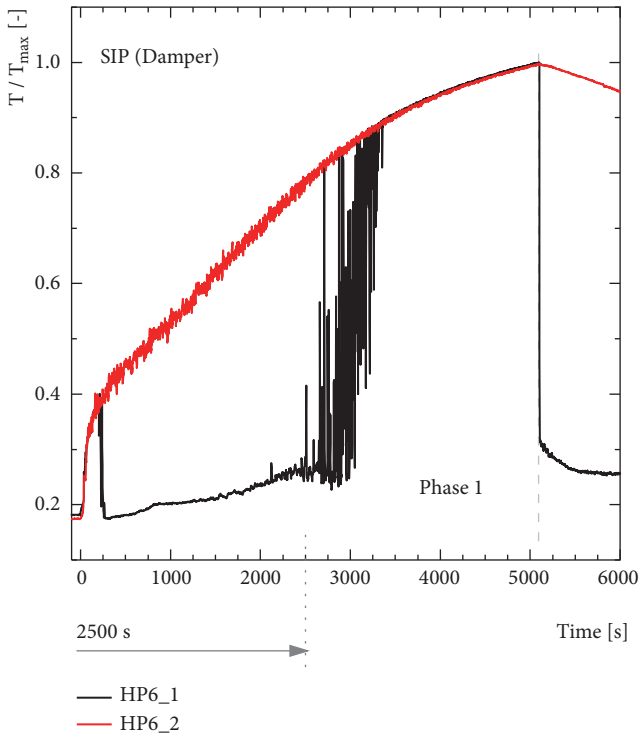


Figure 4: Normalized temperature signal at the orifice (SIP.1 in Figure 3) for experiments HP6_1 and HP6_2. Temperature is normalized with maximum temperature.

(HP6_2) of an opening in the lower interconnecting pipe between Vessels 3 and 4; see Figure 2.

## 3. Results and Discussions

The complex results of the experiments HP6_1 and HP6_2 will be discussed on the following pages in terms of the damper temperatures, the density and mass inventory, and graphs illustrating the global flow structures. Finally with a Shapiro diagram depicting the flammability risk if helium would have been replaced with hydrogen. The discussion is structured by the four experimental phases as described above and the phenomena in the four vessels starting with Vessel 4 where the steam (phase 1) and later the helium (phase 3) are injected. The molar fraction of steam in the entire Vessel 4 increases during phase 1 of the experiment from 0 to almost 1, Figure 7. Since the steam jet is injected horizontally (Figures 2 and 3) with a high velocity it is expected that it impinges onto the opposite vessel wall and deflects towards the lower and upper part of the vessel, Figure 8(a). By using the temperature recorded at the orifice we find for HP6_1 – except for the small spike right after the opening of the valve for the steam release, initially (up to $\approx 2500\ s$) a temperature close (i) to the initial conditions in the vessels and (ii) close to the Vessel 3 temperatures, while experiment HP6_2 (with the closed orifice which avoids a flow between Vessel 3 and 4 as well as vice versa) shows a fast temperature increase, Figure 4.

Thus it is concluded that there is a flow from Vessel 3 to Vessel 4 during the first 2500 s of the experiment (excluding the first 100-200 s). This flow is reversed during the second part of phase 1, Figure 8(b). Beyond 2500 s a fast steam content increase is monitored at the orifice for HP6_1 (not shown) which results from a convective transport from Vessel 4 to Vessel 3 through the pipe since the steam content in Vessel 3 is almost zero (initial condition was pure air), see also Figure 8(b). Using the gas composition (air, helium, and steam), the temperature, and the pressure, it is possible to calculate the gas density around each sensor locations. Selected results for this calculation as a function of time are depicted in Figure 5. The gas composition in the lines VB2 and MV2 which connect Vessels 4 and 2 are almost identical during phase 1 which results in the same density (Figure 5) and this statement holds true for the entire experiment HP6_1. Except for the initial part of phase 1, there is a strong correlation between the gas density close to the pipe inlet in Vessel 4 (measurement location GS2_25) and the measurements in the pipe close to the pipe exits (MV2 and VB2), i.e., whatever gas composition we find at the pipe inlet is also found—with some delay—at the pipe outlet. Both phenomena indicate a flow through both pipes from Vessel 4 to Vessel 2.

Once the steam injection is stopped (phase 2 after 5100 s) the steam content in Vessel 4 decays such that at lower positions it drops earlier than at upper positions, Figure 7; i.e., the steam in Vessel 4 is removed like a piston moves in a motor from the bottom to the top, Figure 8(c). Together with the sensor positions (Table 1) this allows for an estimate of the volumetric flow rate and the corresponding velocities at the damper and in the pipes VB2, MV2 and VB1 as follows. Neglecting condensation, the steam 'piston' moves on average by $\approx 1\,\text{m}/300\,\text{s}$. By using the vessel radius $r = 2\,\text{m}$ this corresponds to a volume of $V \approx 12\,m^3$ or a volumetric flow rate of $\dot{V} \approx 0.04\,m^3/s$. With the radius of the rupture disk $r = 0.04\,\text{m}$ it follows $u = \dot{V}/A \approx 8\,\text{m/s}$ at this location. With the radius $r = 0.067\,\text{m}$ for the pipe VB1 one obtains $u \approx 2.8\,m/s$ and with $r_{VB2} \approx r_{MV2}$ we have approximately $u \approx 1.4\,\text{m/s}$ in both pipes.

For each vessel one upper and one lower position were selected to present the overall gas transport between the four vessels. Additionally we present the sensors located in the pipes connecting different parts of the vessels. By using the gas densities we can now distinguish two subphases during phase 2 for experiment HP6_1. Initially (5100 to 6950 s), the gas density leaving VB2 (MV2) is lower than the density in the upper part of Vessel 2 (D2B_15). The jets leaving VB2 (MV2) can only penetrate partially into the upper part of Vessel 2, Figure 8(c). But later (still during phase 2: 6959 to 8100 s) we find a situation where the gas density leaving VB2 (MV2) becomes higher than the gas density in the top part of Vessel 2 (D2B_15), Figure 5 mark A. Consequently, the jets emerging from VB2 and MV2 can not penetrate anymore into the upper gas atmosphere in Vessel 2. Thus, it is expected that the jet flow is deflected and redirected into the IP between Vessels 2 and 1; see Figure 8(d). During phase 2 (6950 to 8100 s), the density in the upper part of Vessel 1 (D1C_26) remains higher than the gas density emerging from the IP such that the gas partially penetrates into the upper part and

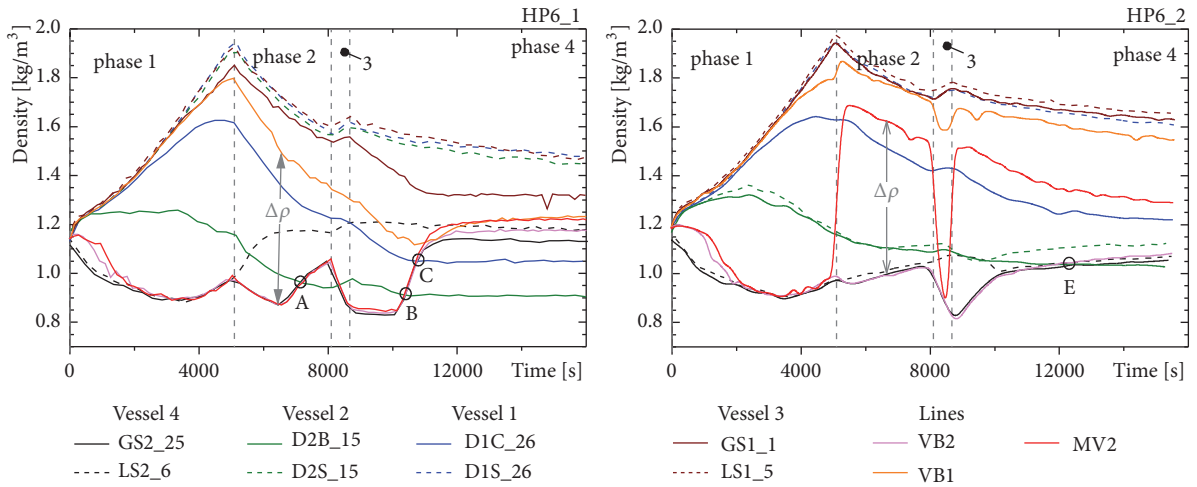


Figure 5: Density as a function of time for selected locations in all for vessels for experiments HP6_1 (left) and HP6_2 (right). Legend nomenclature refers to locations depicted in Figure 3.

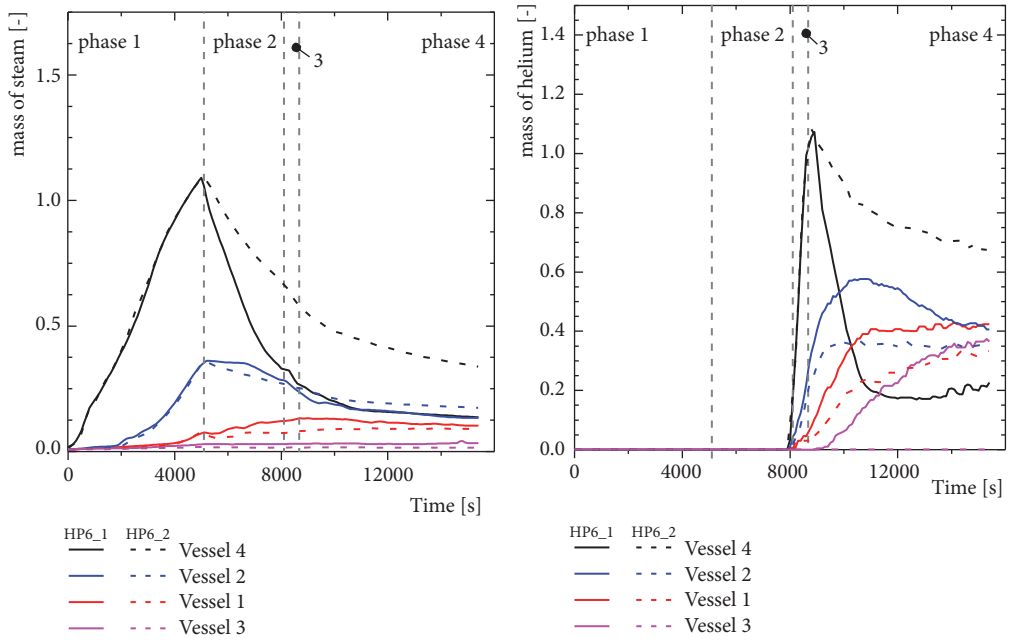


Figure 6: Steam (left) and helium (right) mass inventory in all of the four PANDA vessels as a function of time for experiment HP6_1 and HP6_2. Masses are presented in arbitrary units.

the resulting mixture from the convection loop enters VB1, Figure 8(d).

During phase 3 of the experiment helium is injected into Vessel 4, Figure 6. Consequently, the density in the upper part of Vessel 4 decreases, but not in the lower part below the injection level, Figures 5 and 8(e). The helium leaves Vessel 4 through VB2 and MV2 which both show the same helium content, Figure 8(e). As for the steam injection phase we find also for the helium injection a strong correlation between the gas density close to the pipe inlets in Vessel 4 (measurement location GS2_25) and the pipe exits; i.e., the helium content at this location predicts (with a small delay) the helium content at the pipe outlet. Finally, during phase 4 of the experiment (no steam and no helium injection), the remaining helium in Vessel 4 is convected (up to 10700 s, mark C in Figure 5) into Vessel 2 like a helium rich gas piston which moves upwards such that the helium molar fraction for lower sensor positions decay earlier compared to upper sensor positions, Figure 8(f). The helium content of VB2 decays very fast past 10700 s but the helium content in the upper parts of Vessels 2 and 1 remains almost constant (not shown). This can be explained as follows. The helium rich gas released to Vessel 2 initially penetrates into the upper parts of Vessel 2 and the helium content still increases there for some time even after the helium injection was stopped, Figure 8(f). The helium rich gas is released during 8600 to 10700 s from Vessel 4

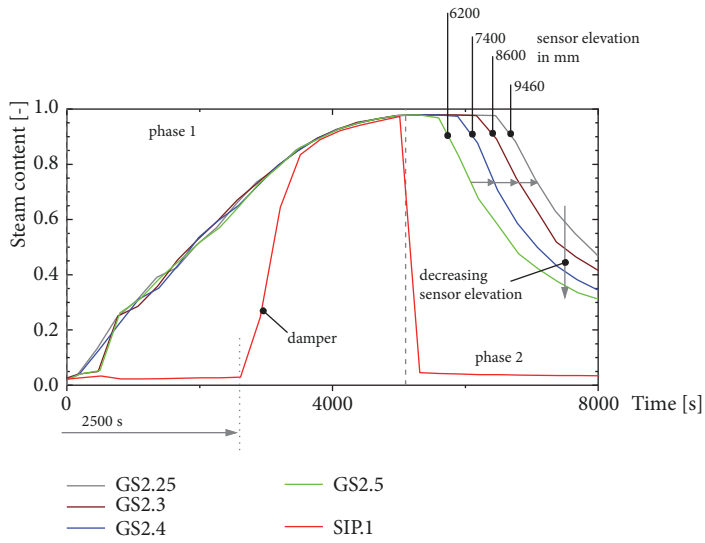


Figure 7: Steam content in Vessel 4 for experiment HP6_1.

Table 1: Characteristic data to calculate the flow rate at different locations.

| sensor | elevation [$mm$] | $t$ [$s$] | $c_{steam}$ - | $\Delta x$ [$mm$] | $\Delta t$ [$s$] |
|---|---|---|---|---|---|
| GS2.5 | 6200 | 6200 | 0.68 | | |
| GS2.4 | 7400 | 6480 | 0.71 | 1200 | 280 |
| GS2.3 | 8600 | 6770 | 0.75 | 1200 | 290 |
| GS2.25 | 9460 | 7050 | 0.75 | 860 | 280 |

which acts as a kind of reservoir. Part of the helium is then transported (with some delay) through the IP to Vessel 1 with a corresponding (smaller) increase of the helium content in the upper part and no helium increase is monitored in the lower parts of Vessel 2 and 1.

By again using the gas densities we can also distinguish two subphases during phase 4. Initially, the gas density leaving VB2 (MV2) is lower than the gas density in the upper part of Vessel 2 (Figure 5) but later the gas density becomes higher (mark B) than the gas in the top of Vessel 2 and the density becomes even higher than the density in the upper part of Vessel 1 (mark C). From this time on (past 10700 s) penetration is neither possible into the upper parts of Vessels 2 nor possible into the upper parts of Vessel 1 (Figure 8(g)) and the global flow structure through all 4 vessels is confined to the flow paths pictured in Figure 8(h) such that the upper parts of Vessel 2 and 1 remain untouched by the natural circulation flow. Consequently, the concentrations of helium (and even steam) remain in these parts almost unchanged until the end of the experiment. The essential driving force for the natural circulation during phase 4 are the gas mixture density differences (considering gas composition, pressure, and temperature) as depicted in Figure 5 which are caused by temperature differences between the four vessels as shown in Figure 9 for $t = 12000\ s$ with temperature maps for Vessels 1 and 2 as well as gas and wall temperatures in Vessels 3 and 4. Through the steam injection during phase 1 mainly Vessel 4 was heated up while we find only a moderate temperature increase above the initial ambient conditions in Vessel 3. The temperature stratification in the top parts of Vessels 1 and 2 with a higher temperature signature in Vessel 2 are caused through the gas transport during the previous phases of the experiment where the gas flow could reach these locations as discussed above.

Using the gas composition for all four vessels at different elevations and assuming no or neglectable horizontal composition gradients it is possible to calculate the integral mass of the three-gas species (steam, air, and helium) for each vessel separately during the course of the experiment. This highlights the phenomena and the gas transport between the four vessels from another perspective. The results for helium and steam are presented in Figure 6 in arbitrary units. Initially all four vessels are filled with air. This air is almost completely removed from Vessel 4 during phase 1 (steam injection), i.e., the air atmosphere is replaced by a steam atmosphere. The air removed from Vessel 4 is transported mainly to Vessels 3 and 1 and to a smaller extent to Vessel 2. The latter is because the air atmosphere in Vessel 2 is—to a certain extent—also replaced by steam since Vessel 2 and 4 are directly connected by two pipes (VB2 and MV2). From another perspective, there is almost no transport of steam into Vessel 3 and little transport into Vessel 1. During phase 2 the steam mass decays in Vessels 4 and 2 through condensation and increases slightly in Vessel 1 through transport. Finally, during and after the helium injection (phases 3 and 4), the helium is mainly transported into the upper parts of Vessels 2 and 1 and remains there; i.e.,

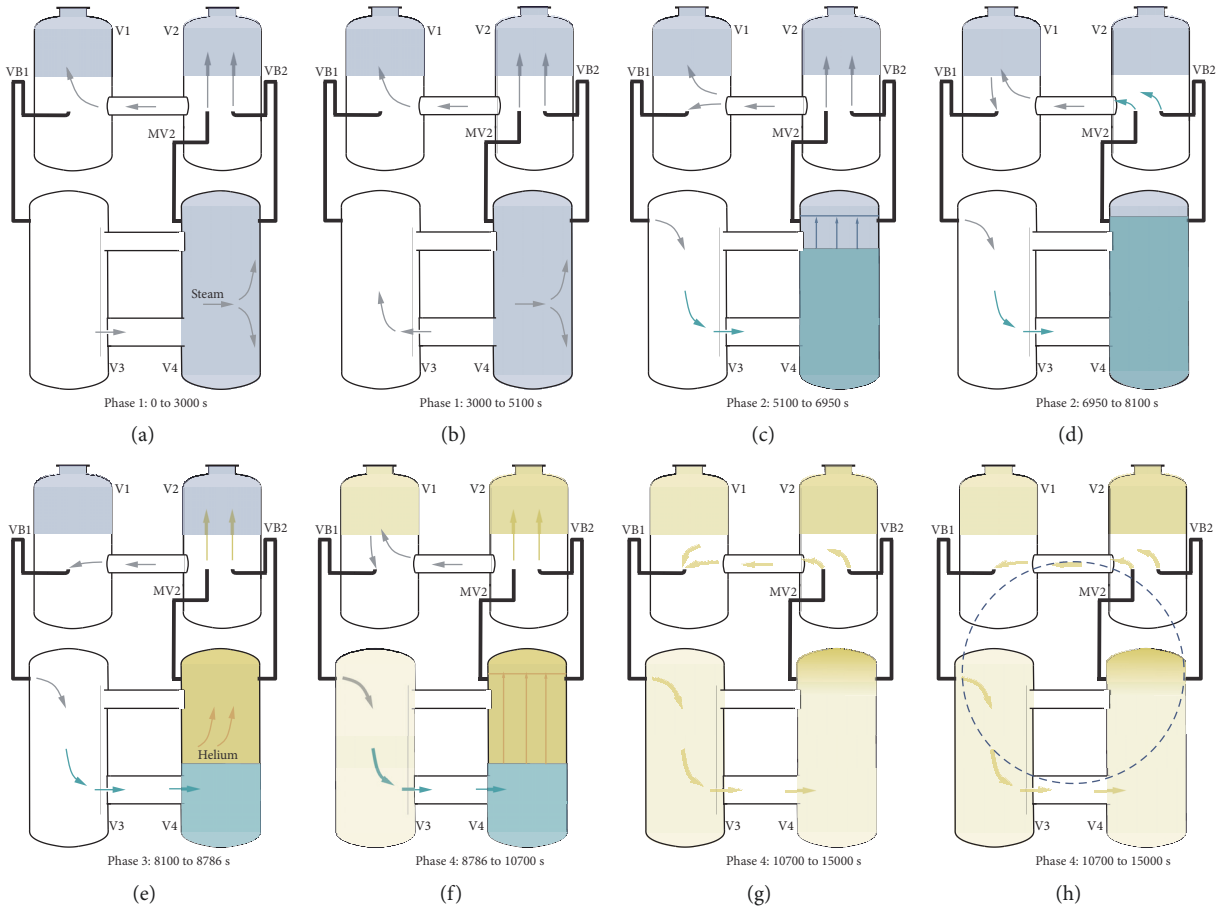


Figure 8: Global flow structures and phenomena in all four vessels during all phases of the experiment HP6_1.

the final natural circulation loop does not affect these parts of both Vessels 1 and 2 such that a strong helium stratification is kept trapped, Figure 6. With some delay towards the end of the experiment, helium is also transported into Vessel 3 such that we finally find a higher mass of helium in Vessel 3 compared with Vessel 4.

For experiment HP6_2 Vessel 3 and Vessel 4 are not connected at all, i.e., the small orifice in the lower interconnecting pipe representing an open damper—which would allow flow between Vessels 3 and 4—is closed, Figure 2. Similar to experiment HP6_1, the molar fraction of steam in the entire Vessel 4 increases during phase 1 of the experiment from 0 to almost 1. Since the steam jet is injected horizontally it is again expected that it impinges onto the opposite vessel wall and deflected towards the lower and upper part of the vessel resulting in a good mixing of the gas in the vessel, Figure 10(a). The gas composition in VB2 and MV2 which connect Vessels 4 and 2 are almost identical during phase 1, but this statement does not hold true for the rest of the experiment, which is in contrast to the findings for HP6_1; see Figure 5 left and right. When the steam injection is stopped (phase 2 of the experiment after 5100 s) the steam content in Vessel 4 decays continuously and irrespective of sensor position; i.e., there must be a strong mixing mechanism present which acts in the entire vessel, except for the sensor location above the inlet of VB2 and MV2. This is in contrast to the observations for experiment HP6_1.

Immediately after the steam injection was stopped for experiment HP6_2, the steam content in MV2 drops rapidly to almost zero while VB2 closely follows the concentration in the upper part of Vessel 4. From this observation we can conclude that the flow direction in MV2 changes sign as soon as the steam injection is stopped, Figure 10(b), which is also a major difference to experiment HP6_1. During phase 2 the gas density flowing downwards in MV2 remains always much heavier than the gas in Vessel 4, even though the density difference becomes smaller in time, Figure 5-right. Consequently, the gas stream entering Vessel 4 will flow almost to the bottom of Vessel 4 and will induces a large scale circulation while mixing with the surrounding gas in the entire vessel, Figure 10(b). Since the gas entering MV2 is much heavier than the gas in the top part of Vessel 2 (sensor location D2B_15 in Figure 5) the origin of the gas entering MV2 must be at an intermediate level between the top and bottom part of Vessel 2; a location approximately located at the level of the interconnecting pipe. Consequently, it is reasonable to assume a flow in the interconnecting pipe from Vessel 1 to Vessel 2 such that gas with an intermediate density from Vessel 1 also contributes to the overall flow structure Figure 10(c). This flow from Vessel 1 to Vessel 2 requires also

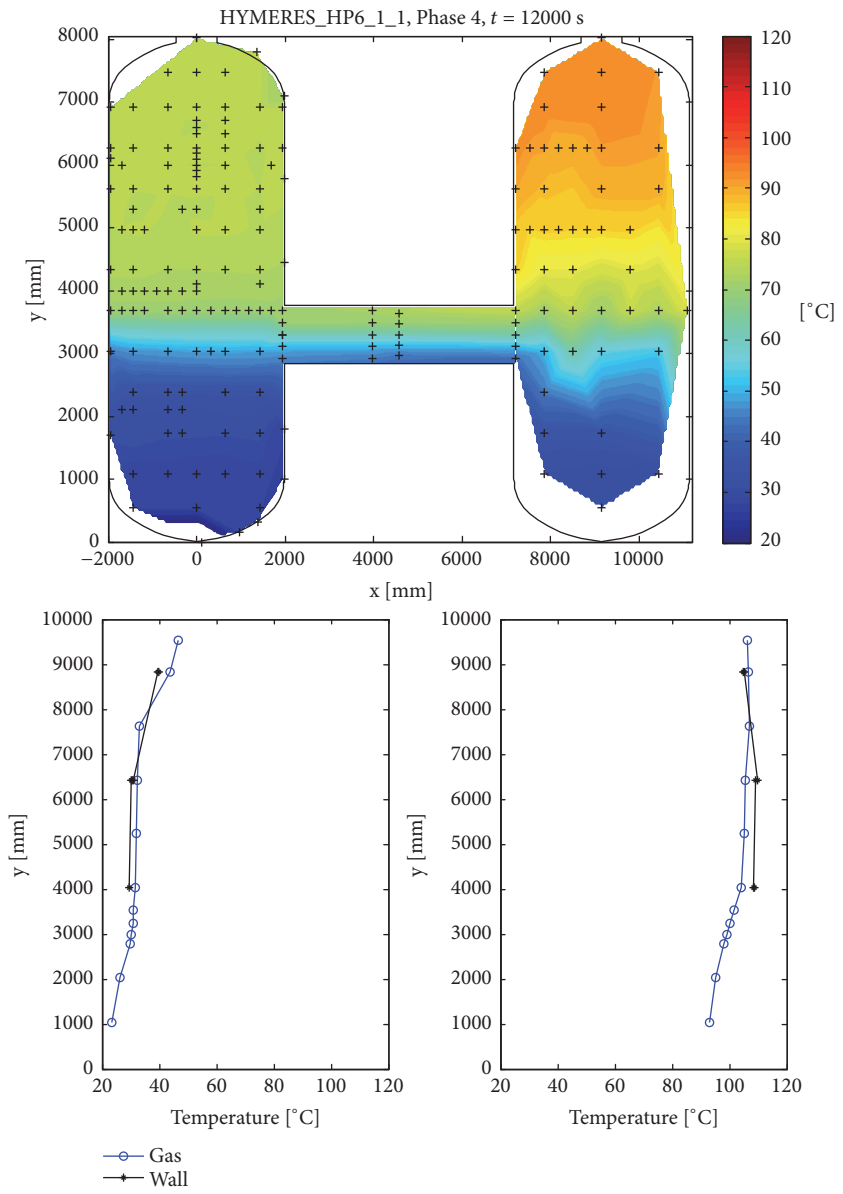


Figure 9: Temperature maps for Vessels 1 and 2 as well as gas and wall temperatures in Vessels 3 and 4 for experiment HP6_1 at $t = 1200$ $s$.

a corresponding flow from Vessel 3 to Vessel 1 as depicted in Figure 10(c). The flow reversal in VB1 from Figures 10(b) and 10(c) is deduced from the mass balance where we monitor a weak air mass decay in Vessel 3 (not shown).

During phase 3 of the experiment helium is injected into Vessel 4. As for experiment HP6_1, the helium content in the upper part of Vessel 4 increases, but not in the lower part below the injection level (4960 mm), Figures 3 and 10(d). The helium leaves Vessel 4 through both VB2 and MV2 which show the same helium content, i.e., compared with phase 2 the flow through MV2 is again reversed.

Finally, during phase 4 of the experiment (no steam and no helium injection), the helium content in the upper part of Vessel 4 decays and remains well mixed in the volume between the injection level (4960 mm) and the inlet level (GS2_25, 9460 mm) of VB2 and MV2 (Figure 3). This is fundamentally different from the helium decay characteristics monitored during HP6_1. Similar to experiment HP6_1, the helium rich gas released through VB2 into Vessel 2 initially penetrates into the upper parts of Vessel 2 and the helium content still increases there for some time even after the helium injection was stopped, Figure 10(e). This is confirmed by the densities presented in Figure 5. The gas released through VB2 is (initially) lighter than the gas in the upper part of Vessel 2 and this holds true up to mark E in Figure 5. From this time on ($\approx 12000$ s) the gas leaving VB2 can not penetrate anymore into the upper part of Vessel 2 and we monitor a circulation of the flow mainly between Vessel 4 and Vessel 2, Figure 10(f). The presence of the damper has a strong effect on the resulting helium content after the experiment in the

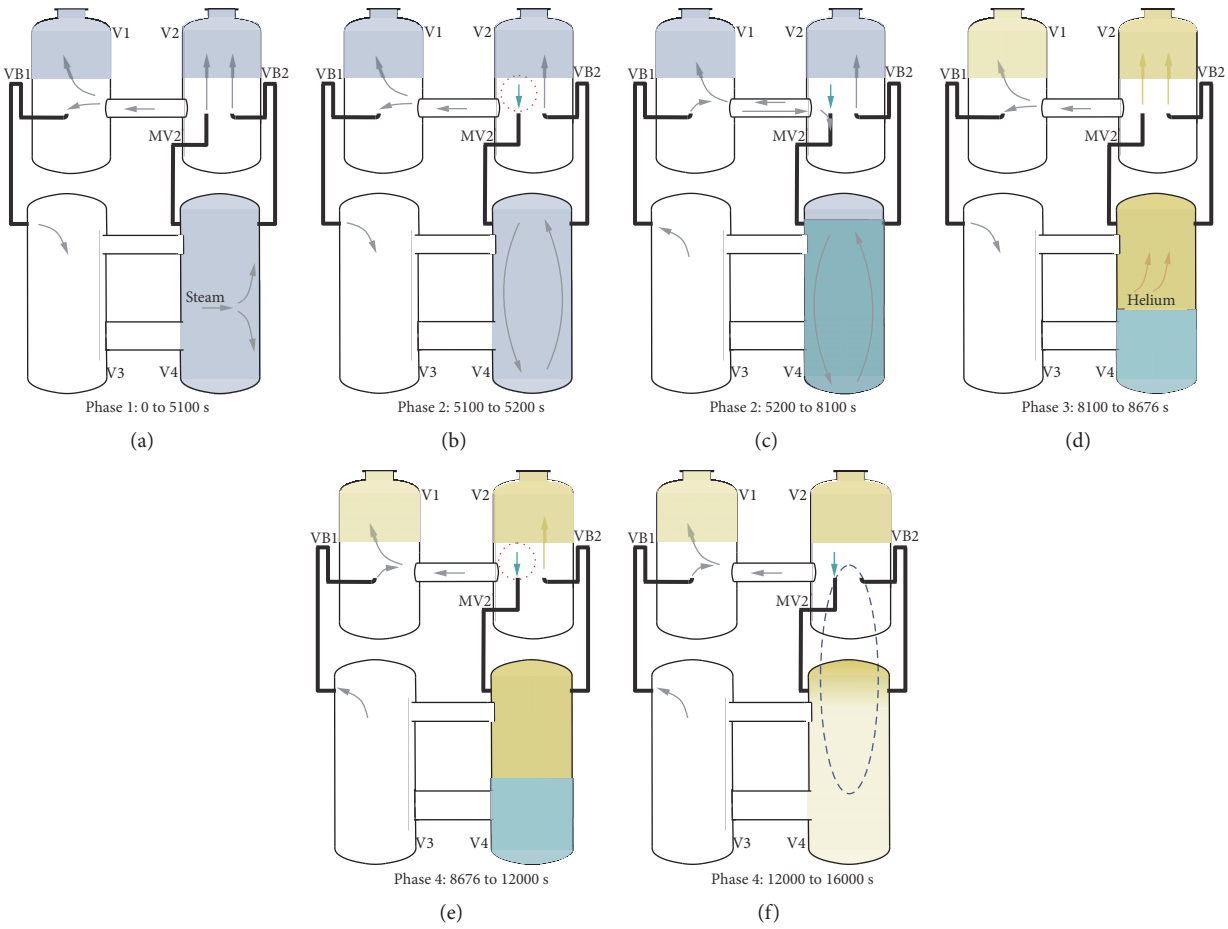


Figure 10: Global flow structures and phenomena in all four vessels during all phases of the experiment HP6_2.

inner zone represented by Vessel 1 (Figure 6) with 3 times less helium compared with the configuration without damper.

The composition of the three-gas mixture (steam-air-helium) during (phase 3) and after (phase 4) helium injection is presented in a so called Shapiro diagram (see [12–14]) for all four vessels, for a lower and upper position, Figure 11. For the flammability risk the helium is treated as if it were hydrogen and the flammability limit depicts ambient conditions, i.e., 24°C and 1 bar according Shapiro and Moffette [12]. The Shapiro diagram combines selected data from phases 3 and 4 into one diagram. The data from the steam, air, and helium molar fraction for a specific time result into one point such that the traces of these points show initially (during phase 3 and the beginning of phase 4) a stronger variation compared with a later state when the respective data approach almost steady state conditions. The Shapiro diagram shows for experiment HP6_1 on the one hand that the maximum for Vessel 4 is inside the flammability limit for a period of time and on the other hand that this region is also left again in the further course of the experiment, Figure 11(left). More critical (in terms of flammability) is the gas mixture in the upper parts of Vessels 1 and 2, which remained untouched from the final natural circulation pattern forming in all vessels as discussed above. These compositions cross the flammability limit and remain in this region until the end of the experiment. The Shapiro diagram for HP6_2 shows that the maximum for helium/hydrogen in Vessel 4 is outside the flammability limit, Figure 11(right). The gas mixtures in Vessels 4, 2, and 1 all cross finally the flammability limit and remain in this region until the end of the experiment, but remain much closer to this limit compared with experiment HP6_1 where we found much higher helium concentrations in the upper part of Vessel 2 and 1.

## 4. Conclusions

The experiments presented in this paper consider natural circulation flow in a two-room type containment. The results showed that a generic two-room containment (TRC) mixing scenario can be well represented with the PANDA facility. For experiment HP6_1 Vessel 3 and Vessel 4 were connected by a small orifice in the lower interconnecting pipe which represents an open damper. During the first half of the steam injection phase (phase 1) we found evidence for a flow from Vessel 3 to Vessel 4 while the flow direction changes (flow from Vessel 4 to Vessel 3) during the second half of the steam injection. With the calculated density it was possible

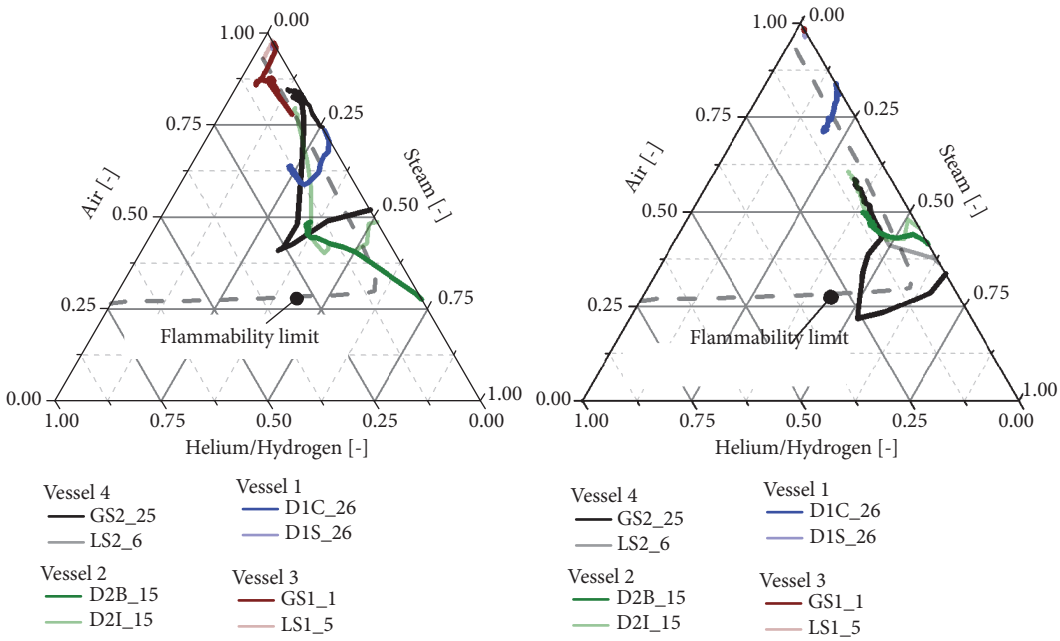


Figure 11: Shapiro diagram with flammability limit for helium (hydrogen)-air-steam mixtures at 1 bar for experiment HP6_1 (left) and HP6_2 (right).

to identify two subphases during phase 2. Initially, the gas leaving MV2 and VB2 can penetrate partially into the upper part of Vessel 2 while later the gas becomes too heavy and the available momentum does not allow for the penetration such that the gas stream is deflected towards the interconnecting pipe. Again with the calculated densities we could detect also two subphases during phase 4. Initially, the gas density leaving VB2 (MV2) is lower than the gas density in the upper part of Vessel 2 but later the gas density becomes higher than the gas in the top of Vessel 2 and the density becomes even higher than the density in the upper part of Vessel 1. Consequently, during and after the helium injection (phases 3 and 4), the helium is mainly transported into the upper parts of Vessels 2 and 1 and remains there; i.e., the final natural circulation loop does not affect these parts of both Vessels 1 and 2 such that a strong helium stratification is kept trapped. With a Shapiro type diagram it was proven that the gas composition in the upper parts of Vessel 2 and 1 (i) cross the flammability limit if the helium content would have been hydrogen and (ii) remain in this region until the end of the experiment. For experiment HP6_2 Vessel 3 and Vessel 4 were not connected; i.e., the orifice in the lower interconnecting pipe was closed. The gas composition (and therefore the densities) in VB2 and MV2 which connects Vessels 4 and 2 is almost identical during phase 1. This indicates a flow through both pipes from Vessel 4 to Vessel 2. The gas leaving Vessel 4 is transported towards the upper part of Vessel 2 and almost no gas is transported towards the lower part. Part of this gas is then transported through the IP in the upper part of Vessel 1 but there is almost no transport of steam into Vessel 3. Immediately after the steam injection was stopped (phase 2) the steam content in MV2 drops rapidly to almost zero while VB2 closely follows the concentration in the upper part of Vessel 4. From this observation we concluded that the flow direction in MV2 changes sign as soon as the steam injection is stopped. The gas density flowing downwards in MV2 remains always much heavier than the gas in Vessel 4. Consequently, once entering the Vessel 4 it will flow almost to the bottom of Vessel 4 and induces a large scale circulation while mixing with the surrounding gas in the entire vessel. It is reasonable to assume a flow in the interconnecting pipe from Vessel 1 to Vessel 2 as well as a counter-current flow in the IP connecting Vessels 1 and 2. One flow path feeding the heavy gas to MV2 (flow from Vessel 1to Vessel 2) and another flow increasing the steam molar fraction in Vessel 2 (flow from Vessel 2 to Vessel 1). Similar to experiment HP6_1, the helium rich gas released through VB2 into Vessel 2 initially penetrates into the upper parts of Vessel 2 and the helium content still increases there for some time even after the helium injection was stopped. The presence of the damper has a strong effect on the final helium content after the experiment in the inner zone represented by Vessels 1 with 3 times less helium compared with the configuration without damper. In the Shapiro type diagram we found that the gas mixtures in Vessels 4, 2, and 1 all cross finally the flammability limit if the hydrogen would have been used and remain in this region until the end of the experiment but remain much closer to this limit compared with experiment HP6_1 where we found much higher helium concentrations in the upper part of Vessels 2 and 1.

## Data Availability

The data of the OECD HYMERES project belongs to the project participants. The full set of HYMERES experimental

data will be opened for the public in 2020. Moreover, if the reader is from one of the HYMERES participating countries and would like to analyse the PANDA HP6 tests with computational tools, he/she could contact the project representative organization in his/her own country and/or the OECD/NEA to obtain additional information related to the HYMERES PANDA HP6 tests and project documents.

## Conflicts of Interest

The authors declare that they have no conflicts of interest.

## Acknowledgments

The authors gratefully acknowledge the technical contribution of Max Fehlmann (PSI) and Simon Suter (PSI) and the support from the PRG (PSI) and MB of the HYMERES project.

## References

[1] M. Andreani, A. Badillo, and R. Kapulla, "Synthesis of the OECD/NEA-PSI CFD benchmark exercise," *Nuclear Engineering and Design*, vol. 299, pp. 59–80, 2016.

[2] OECD-NEA, "NEA Hydrogen Mitigation Experiments for Reactor Safety (HYMERES) Project," 2016, https://www.oecd-nea.org/jointproj/hymeres.html.

[3] D. C. Visser, N. B. Siccama, S. T. Jayaraju, and E. M. J. Komen, "Application of a CFD based containment model to different large-scale hydrogen distribution experiments," *Nuclear Engineering and Design*, vol. 278, pp. 491–502, 2014.

[4] H. Dimmelmeier, J. Eyink, and M.-A. Movahed, "Computational validation of the EPR™ combustible gas control system," *Nuclear Engineering and Design*, vol. 249, pp. 118–124, 2012.

[5] M. Andreani, D. Paladino, and D. Papini, "Multi-step planning calculations with the GOTHIC code used for the design of a complex experiment," in *NURETH-17*, Qujiang, China, September 2017.

[6] S. Kelm, R. Kapulla, and H.-J. Allelein, "Erosion of a confined stratified layer by a vertical jet – Detailed assessment of a CFD approach against the OECD/NEA PSI benchmark," *Nuclear Engineering and Design*, vol. 312, pp. 228–238, 2017.

[7] R. Kapulla, G. Mignot, S. Paranjape, L. Ryan, and D. Paladino, "Large scale gas stratification erosion by a vertical helium-air jet," *Science and Technology of Nuclear Installations*, vol. 2014, Article ID 197267, 16 pages, 2014.

[8] R. Kapulla, G. Mignot, and D. Paladino, "Large-scale containment cooler performance experiments under accident conditions," *Science and Technology of Nuclear Installations*, vol. 2012, Article ID 943197, 20 pages, 2012.

[9] D. Paladino, M. Andreani, R. Zboray, and J. Dreier, "Toward a CFD-grade database addressing LWR containment phenomena," *Nuclear Engineering and Design*, vol. 253, pp. 331–342, 2012.

[10] D. Papini, M. Andreani, B. Niceno, H.-M. Prasser, P. Steiner, and J.-U. Kluegel, "Simulation of hydrogen distribution in the containment during a severe accident with fast hydrogen-steam release," in *NURETH-16*, Chicago, IL, USA, August 2015.

[11] A. Filippov, S. Grigoryev, N. Drobyshevsky, A. Kiselev, A. Shyukin, and T. Yudina, "CMFD simulation of ERCOSAM PANDA spray tests PE1 and PE2," *Nuclear Engineering and Design*, vol. 299, pp. 81–94, 2016.

[12] Z. M. Shapiro and T. R. Moffette, "Hydrogen Flammability Data And Application To Pwr Loss-Of-Coolant Accident," Tech. Rep., Bettis Plant Pittsburgh, Pensilvania, 1957, WAPD–SC-545.

[13] A. Slide and I. Lindholm, "On Detonation Dynamics in Hydrogen-Air-Steam Mixtures: Theory And Application to Oikiluoto Reactor Building," Tech. Rep., 2000, VTT.

[14] A. Bentaib, N. Meynet, and A. Bleyer, "Overview on hydrogen risk research and development activities: Methodology and open issues," *Nuclear Engineering and Technology*, vol. 47, no. 1, pp. 26–32, 2015.